2014

Development of a Lumped-Parameter Model for Hermetic Reciprocating Compressor with Thermal-Electrical Coupling

Thiago Dutra
POLO/ Federal University of Santa Catarina, Brazil, dutra@polo.ufsc.br

Cesar J. Deschamps
POLO/ Federal University of Santa Catarina, Brazil, deschamps@polo.ufsc.br

Development of a Lumped-Parameter Model for Hermetic Reciprocating Compressor with Thermal-Electrical Coupling

Thiago DUTRA, Cesar J DESCHAMPS*

POLO Research Laboratories for Emerging Technologies in Cooling and Thermophysics
Federal University of Santa Catarina
Florianópolis, SC, Brazil
dutra@polo.ufsc.br, deschamps@polo.ufsc.br

*Corresponding Author

ABSTRACT

The design of high-efficiency reciprocating compressors requires good understanding of interactions between different phenomena inside the compressor. This paper describes a comprehensive model to predict the performance of reciprocating compressors with thermal-electrical coupling. The simulation of the compression cycle is based on an integral control volume formulation for mass and energy conservation. The thermal model follows steady state thermal energy balances applied to the compressor components by using global thermal conductances. Finally, the equivalent circuit method is employed to simulate a steady-state model of single-phase induction motor. The motor losses are used as heat generation in the energy equation of the thermal model, which in turn provides the motor temperature required to evaluate the windings resistances. Predictions are compared to experimental data under different operating conditions and reasonable agreement is observed.

1. INTRODUCTION

Different phenomena take place inside compressors, encompassing thermodynamic, heat transfer and electromagnetic processes and therefore multi-physics modeling is required for comprehensive simulations. For instance, the use of a model for the induction motor allows one to predict the electromagnetic effect on both heat transfer and the compression cycle. Furthermore, this approach allows the compressor simulation model to be less dependent on experimental data to describe the motor performance.

There are several methods to simulate the compression cycle, such as prescription of polytropic processes (Cavallini *et al.*, 1996; Chikurde *et al.*, 2002), lumped-parameter model (Todescat *et al.*, 1992; Rigola *et al.*, 2000) or distributed-parameter model (Birari *et al.*, 2006). Different modeling techniques are also employed to predict the temperature distribution inside the compressor. Steady state lumped-parameter methods are common practices, with thermal conductances between elements being obtained from experimental data (Todescat *et al.*, 1992) or from classical heat transfer correlations (Ooi, 2003). The finite volume method (FVM) is also employed to solve fluid flow and heat transfer equations (Raja *et al.*, 2003; Birari *et al.*, 2006), therefore without requiring prescription of thermal conductances. Recently, hybrid models have been developed by combining lumped formulation for the fluid domain and FVM for solving heat conduction in solid elements (Ribas Jr., 2007; Sanvezzo Jr. and Deschamps, 2012). Hybrid models are less computationally demanding than full-based FVM and can better describe heat transfer in solid components than lumped-parameter models. All the aforementioned models include motor losses in the thermal model via relations between torque, efficiency and compressor speed obtained from experimental data or theoretical estimates.

Thermal-electrical models applied to electrical motors are available and may combine lumped-parameter thermal models with equivalent circuit methods for electrical models (Mellor *et al.*, 1991; Eltom and Moharari, 1991) or adopt finite element method for both thermal and electrical models (Hwang *et al.*, 2000; Li *et al.*, 2010). On the other hand, few works have applied thermal-electrical models in the simulation of compressors. Peruzzi *et al.* (1980)

employed a thermodynamic-thermal-electrical model as a design tool to assess proposals of efficiency improvement for a reciprocating compressor. He *et al.* (2013) presented a simulation model for a semi-hermetic screw compressor with the equivalent circuit method for the thermal and electrical modeling.

The present paper reports the development of a thermodynamic-thermal-electrical model to predict the performance of reciprocating compressors. The thermodynamic and thermal models adopted to simulate the compression cycle and the temperature distribution employ the lumped-parameter method, whereas the electrical model is based on a motor equivalent circuit. Predictions for compressor efficiency and temperature distribution are obtained and compared to measurements.

2. THERMODYNAMIC MODEL

The thermodynamic model adopted to simulate the compression cycle is based on the application of mass and energy balances in the compression chamber by using a lumped-parameter formulation (Todescat *et al.*, 1992):

$$\frac{dm_c}{dt} = \dot{m}_{suc} - \dot{m}_{dis} - \dot{m}_{leak} - \dot{m}_{bdis} + \dot{m}_{bdis} \tag{1}$$

$$\frac{dT_c}{dt} = \frac{1}{m_c c_v}\left\{\dot{Q}_w - h_c\frac{dm_c}{dt} - \sum \dot{m}h - \left[\frac{T_c}{\rho_c}\frac{\partial p_c}{\partial T_c}\bigg|_{\rho}\left(\rho_c\frac{d\forall_c}{dt} - \frac{dm_c}{dt}\right)\right]\right\} \tag{2}$$

where t is time, m_c is the instantaneous mass of gas inside the compression chamber and c_v is the gas specific heat at constant volume. Heat transfer at the cylinder walls, $\dot{Q}_w$, is obtained from a correlation proposed by Annand (1963). The compression chamber volume, $\forall_c$, is written as a function of compressor geometrical parameters (Ussyk, 1984). The pressure during the compression cycle, p_c, is evaluated from a real gas state equation and estimates of density, ρ_c, and temperature, T_c, from Equations (1) and (2). The sum of energy fluxes through suction and discharge ports as well as piston-cylinder clearance is represented by $\sum \dot{m}h$. The dynamics of suction and discharge valves is modeled through a single-degree-of-freedom model (Lopes and Prata, 1997) combined with the concept of effective force area (Soedel, 2007). Valve parameters such as natural frequency, stiffness and damping coefficients are input data. Mass flow rate through suction and discharge ports is determined with reference to isentropic compressible flow through a convergent nozzle (Ussyk, 1984) combined with data for effective flow area (Soedel, 2007). The procedure to estimate leakage through piston-cylinder clearance is detailed in Lilie and Ferreira (1984).

The input data required to simulate the thermodynamic model are the evaporating and condensing temperatures, refrigerant properties and geometrical parameters. The compressor speed is obtained from the electrical model whereas the suction and discharge temperatures are calculated in the thermal model. Specific enthalpies are computed from pressure and temperature values, by using the library REFPROP 7.0 (Lemmon *et al.*, 2002). Equations (1) and (2) are numerically integrated via an explicit Euler method.

3. THERMAL MODEL

A steady state energy balance applied to a generic lumped element "*i*" can be mathematically represented by:

$$\dot{Q}_i - \dot{W}_i = \sum \dot{m}h|_{i,in} - \sum \dot{m}h|_{i,out} \tag{3}$$

where $\dot{Q}_i$ encompasses the heat transfer rate between the element i and the surroundings, as well as the heat generation rate within the element i. The rate of work done by or on i is $\dot{W}_i$, and the energy fluxes into and from the element i are denoted by $\sum \dot{m}h|_{i,in}$ and $\sum \dot{m}h|_{i,out}$, respectively. It should be mentioned that potential and kinetic energy were neglected in Equation (3).

The reciprocating compressor was divided into eight lumped elements, corresponding to the following components: suction muffler (1), compression chamber (2), discharge chamber (3), discharge muffler (4), discharge tube (5), electrical motor (6), internal environment (7) and compressor housing (8). The internal environment represents the

portion of refrigerant gas inside the compressor housing. A schematic view of the lumped elements and the thermal interaction among them is depicted in Figure 1, with different arrows adopted to identify the different types of energy transfer.

Equation (3) is applied to all lumped elements giving rise to a system of non-linear equations, which is iteratively solved via Newton-Raphson method. Table 1 shows the corresponding terms of each equation. Convective heat transfer between the compressor internal environment (7) and the other components is taken into account by introducing global conductances, *UA*, obtained from a set of temperature measurements (Todescat *et al.*, 1992). Table 1 indicates that the mass flow rates ($\dot{m}, \dot{m}_{suc}, \dot{m}_{dis}, \dot{m}_{bsuc}, \dot{m}_{bdis}, \dot{m}_{leak}$), the compression power, $\dot{W}_c$, the motor electromagnetic losses ($\dot{Q}_{sta}$, $\dot{Q}_{rot}$ and $\dot{Q}_{iron}$), the mechanical losses in the bearing system, $\dot{W}_b$, the time-averaged specific enthalpy in the cylinder, h_c, and the refrigerant gas mixing factor, φ, must be specified. The mass flow rates, compression power and specific enthalpy are obtained from the solution of the thermodynamic model, whereas the mechanical losses are estimated from measurements and the motor losses are computed from the electrical model. The refrigerant gas mixing factor accounts the proportion of gas mixing in the compressor internal environment, as proposed by Meyer and Thompson (1990). In some compressors, the suction line is directly connected to the suction muffler and there is no mixing between the gas entering through the suction line with the gas in the internal environment; i.e. $\varphi = 1$. In other compressor designs, suction line and suction muffler entrance are misaligned and an amount of the gas entering the compressor flows into compressor internal environment before reaching the suction muffler inlet; hence $0 \leq \varphi < 1$. In the present study, the condition of $\varphi = 1$ was considered.

It should be noted that in Table 1, T_{sm}, $T_{m,dm}$ and $T_{m,dt}$ represent the temperatures in the suction muffler, discharge muffler and discharge tube, respectively. Such temperatures are the arithmetic mean of the gas temperatures at the inlet and outlet of each component. Thus,

$$T_{sm} = 0.5(T_{sl} + T_{sc}); \qquad T_{m,dm} = 0.5(T_{dc} + T_{dm}); \qquad T_{m,dt} = 0.5(T_{dm} + T_{dl}) \tag{4}$$

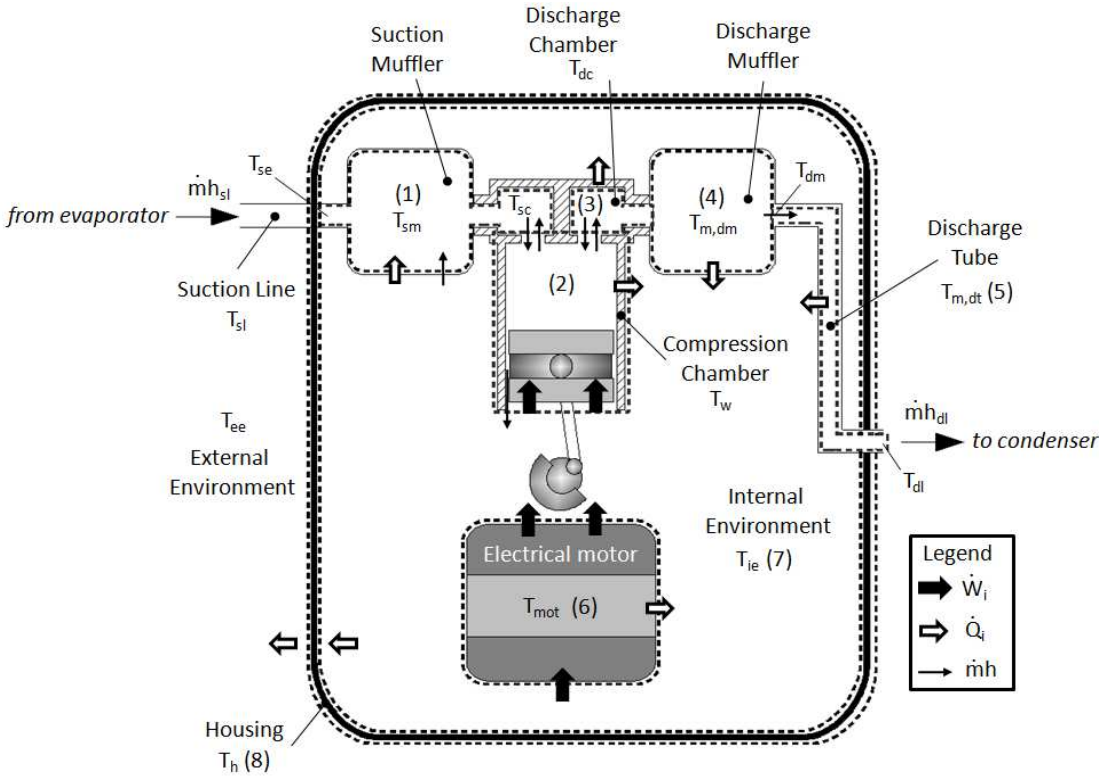

Figure 1: Compressor lumped elements.

Table 1: Energy balance in compressor lumped elements.

Component	$\dot{Q}$	$\dot{W}$	$\dot{m}h\|_{in}$	$\dot{m}h\|_{out}$
1. Suction Muffler	$-UA_{suc}(T_{ie}-T_{sm})$	-	$\dot{m}[\varphi h_{sl}+(1-\varphi)h_{ie}]$ $+\dot{m}_{leak}h_{ie}+\dot{m}_{bsuc}h_c$	$\dot{m}_{suc}h_{sc}$
2. Comp. Chamber	$UA_w(T_w-T_{ie})$	$\dot{W}_c+\dot{W}_b$	$\dot{m}_{suc}h_{sc}+\dot{m}_{bdis}h_{dc}$	$\dot{m}_{leak}h_c+\dot{m}_{bsuc}h_c+\dot{m}_{dis}h_c$
3. Disc. Chamber	$UA_{dc}(T_{dc}-T_{ie})$	-	$\dot{m}_{dis}h_c$	$\dot{m}_{bdis}h_{dc}+\dot{m}h_{dc}$
4. Disc. Muffler	$UA_{dm}(T_{m,dm}-T_{ie})$	-	$\dot{m}h_{dc}$	$\dot{m}h_{dm}$
5. Disc. Tube	$UA_{dt}(T_{m,dt}-T_{ie})$	-	$\dot{m}h_{dm}$	$\dot{m}h_{dl}$
6. Motor	$UA_{mot}(T_{mot}-T_{ie})$ $-(\dot{Q}_{sta}+\dot{Q}_{rot}+\dot{Q}_{iron})$	-	-	-
7. Internal Environment	$UA_{ih}(T_{ie}-T_h)$ $+UA_{suc}(T_{ie}-T_{sm})$ $-UA_w(T_w-T_{ie})$ $-UA_{dc}(T_{dc}-T_{ie})$ $-UA_{dm}(T_{m,dm}-T_{ie})$ $-UA_{dt}(T_{m,dt}-T_{ie})$ $-UA_{mot}(T_{mot}-T_{ie})$	-	$\dot{m}h_{sl}+\dot{m}_{leak}h_c$	$\dot{m}[\varphi h_{sl}+(1-\varphi)h_{ie}]$ $+\dot{m}_{leak}h_{ie}$
8. Housing	$UA_{eh}(T_h-T_{ee})$ $-UA_{ih}(T_{ie}-T_h)$	-	-	-

4. ELECTRICAL MODEL

4.1 Motor Equivalent Circuit

The electrical model of the induction motor was based on a classical approach known as equivalent circuit method. This technique consists on representing the electrical motor in an equivalent circuit with a set of stator (sta), rotor (rot) and magnetizing (m) impedances (Fitzgerald *et al.*, 2006; Hrabovcova *et al.*, 2010). In the present model, stator core electrical resistances are also included in the electrical circuit (iron). Figure 2 shows the equivalent circuit of the single-phase induction motor considered herein.

Rotor and magnetizing parameters are equally divided between the forward (+) and backward (-) branches of the equivalent circuit, following the theory of rotating magnetic fields (Fitzgerald *et al.*, 2006). Therefore, electrical impedances are modeled according to:

$$Z_{sta}=R_{sta}+jX_{sta};\quad Z_{rot}^{+}=0.5R_{rot}^{'}/s+j0.5X_{rot}^{'};\quad Z_{rot}^{-}=0.5R_{rot}^{'}/(2-s)+j0.5X_{rot}^{'} \tag{5}$$

$$Z_m^{+}=j0.5X_m;\quad Z_m^{-}=j0.5X_m;\quad Z_{iron}^{+}=0.5R_{iron};\quad Z_{iron}^{-}=0.5R_{iron} \tag{6}$$

where s is the slip ratio, defined as the relation between the compressor speed, ω, and the synchronous speed, ω_s, $(s=1-\omega/\omega_s)$. The parameter R'_{rot} is the rotor resistance and X'_{rot} is the rotor reactance, both referred to the stator side. The magnetizing reactance and the stator core resistance are represented by is X_m and R_{iron}, respectively. The circuit input impedance, Z_{in}, is given by:

$$Z_{in}=Z_{sta}+\left(\frac{1}{Z_{rot}^{+}}+\frac{1}{Z_m^{+}}+\frac{1}{Z_{iron}^{+}}\right)^{-1}+\left(\frac{1}{Z_{rot}^{-}}+\frac{1}{Z_m^{-}}+\frac{1}{Z_{iron}^{-}}\right)^{-1} \tag{7}$$

where the second and third terms on right hand side of Equation (7) can be interpreted as forward and backward equivalent impedances, Z^{+} and Z^{-}, respectively. Input impedance is used to calculate the *rms* input current, I_{in}:

$$I_{in} = \frac{V_{in}}{Z_{in}} \tag{8}$$

where V_{in} is the *rms* input voltage. Since voltage drop is unique across impedances Z^+, Z^+_{rot} and Z^+_{iron} and also across impedances Z^-, Z^-_{rot} and Z^-_{iron}, the electrical currents in the rotor forward and backward branches, as well as in the stator core, are given by:

$$I^+_{rot} = \frac{IZ^+}{Z^+_{rot}}; \qquad I^-_{rot} = \frac{IZ^-}{Z^-_{rot}}; \qquad I^+_{iron} = \frac{IZ^+}{Z^+_{iron}}; \qquad I^-_{iron} = \frac{IZ^-}{Z^-_{iron}} \tag{9}$$

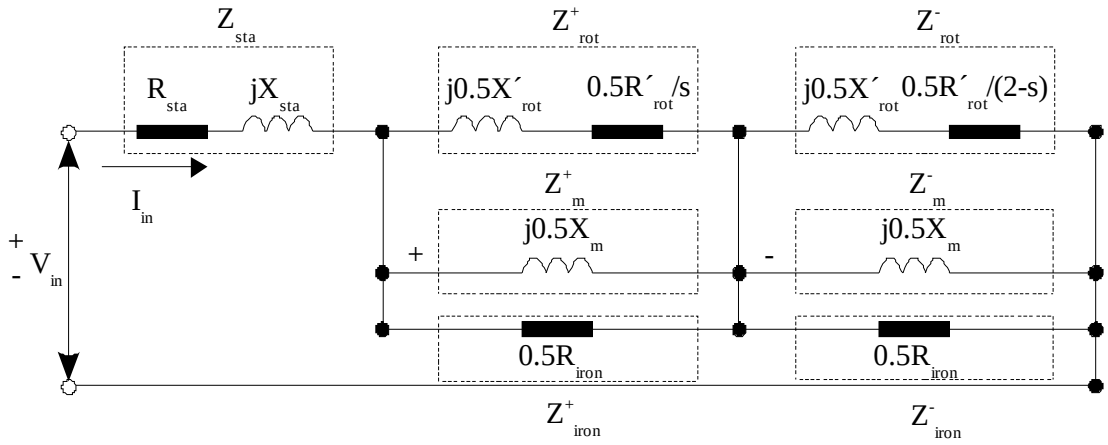

Figure 2: Equivalent circuit of a single-phase induction motor.

According to Huai *et al.* (2003), the losses in the rotor winding, $\dot{Q}_{rot}$, stator winding, $\dot{Q}_{sta}$, and core, $\dot{Q}_{iron}$, account for 75-90% of the motor overall loss. Such losses were set as heat generation rate in the energy equation associated with the motor in the thermal model. The stator winding loss is a function of the stator winding current:

$$\dot{Q}_{sta} = I^2 R_{sta} \tag{10}$$

whereas forward and backward powers arise from the rotating magnetic fields:

$$\dot{W}^+_{rot} = {I^+_{rot}}^2 \frac{0.5R'_{rot}}{s}; \qquad \dot{W}^-_{rot} = {I^-_{rot}}^2 \frac{0.5R'_{rot}}{2-s} \tag{11}$$

and rotor winding loss, $\dot{Q}_{rot}$, is computed as a combination of the forward and backward power components:

$$\dot{Q}_{rot} = s\dot{W}^+_{rot} + (2-s)\dot{W}^-_{rot} \tag{12}$$

Finally, the stator core losses are calculated as a sum of contributions in forward and backward branches:

$$\dot{Q}_{iron} = 0.5R_{iron}\left({I^+_{iron}}^2 + {I^-_{iron}}^2\right) \tag{13}$$

The rate of energy that is not converted into heat is the shaft power, $\dot{W}_{shaft}$, which can be evaluated as the difference between the forward and backward rotating fields powers:

$$\dot{W}_{shaft,e} = (1-s)\left(\dot{W}_{rot}^{+} - \dot{W}_{rot}^{-}\right) \quad (14)$$

The shaft power is delivered to the crankshaft so as to match the energy consumption associated with the compression power and bearings friction losses, $\left(\dot{W}_{shaft} = \dot{W}_c + \dot{W}_b\right)$. For the compressor considered in the present study, bearings friction losses are estimated to be approximately 9W and almost insensitive in relation to the operating condition. Compression power is evaluated from the indicated diagram predicted by the thermodynamic model $\left(\dot{W}_c = -\omega/2\pi \oint p_c d\forall\right)$ and depends on the compressor speed, ω, which is determined in an iterative manner via the coupled simulation of the thermodynamic model and electrical model (Figure 3). Once compressor speed is known, the electromagnetic losses are obtained and used as input data in the thermal model. Finally, the compressor input power and the motor efficiency are calculated:

$$\dot{W}_{in} = \dot{W}_{shaft,e} + \dot{Q}_{sta} + \dot{Q}_{rot} + \dot{Q}_{iron} \quad (15)$$

$$\eta_{mot} = \frac{\dot{W}_{shaft,e}}{\dot{W}_{in}} \quad (16)$$

4.2 Electrical Parameters

The electrical parameters required to solve the equivalent circuit may be obtained via experimental, numerical or analytical approaches. In the present work, electrical resistances and reactances were provided by the compressor manufacturer (Table 2). The assigned values for the stator and rotor winding resistances, R_{sta} and R'_{rot}, correspond to a reference temperature (25ºC). Since electrical resistance varies with temperature, the supplied values must be updated during the simulation according to the expression:

$$R = R_0 + \beta R_0 (T - T_0) \quad (17)$$

where subscript *0* refers to reference state and β is the temperature coefficient. The electrical model also requires input values for voltage and synchronous frequency, which were set to 220V and 50Hz.

Table 2: Electrical parameters.

Stator Winding Resistance (Ω) at 25ºC	11.6
Stator Winding Leakage Reactance (Ω)	16.2
Rotor Winding Resistance - referred to stator side (Ω) at 25ºC	11.0
Rotor Leakage Reactance - referred to stator side (Ω)	4.5
Magnetizing Reactance (Ω)	857
Stator Iron Resistance (Ω)	10,000

5. THERMODYNAMIC-THERMAL-ELECTRICAL COUPLING

The solution algorithm of the thermodynamic-thermal-electrical model is depicted in Figure 3. The procedure starts with input data for geometrical and electrical parameters, as well as operating condition, being specified. Then, the compressor temperature profile is initialized and the electrical resistances are updated. Initially, the slip ratio is set to zero, which means that compressor speed equals synchronous speed. The thermodynamic model is simulated and the shaft power is evaluated. Then, the electrical model is solved and the shaft power is estimated via Equation (14). If the difference of both estimates of shaft power is greater than a specified tolerance, ε_W, the slip ratio is increased by an increment Δs and the simulations are repeated from point identified by '**'. This iterative process is carried out until the convergence defined by the specified tolerance is observed. Once convergence is achieved, output data (mass flow rates, compression power and motor losses) are supplied to the thermal model, which is then simulated to predict the temperature distribution in the compressor components. If the maximum residual found in the energy balances is greater than a specified tolerance, ε_T, the temperatures are updated and calculations start over from point '*'. Otherwise, the simulation is considered to be converged and the solution procedure is finished.

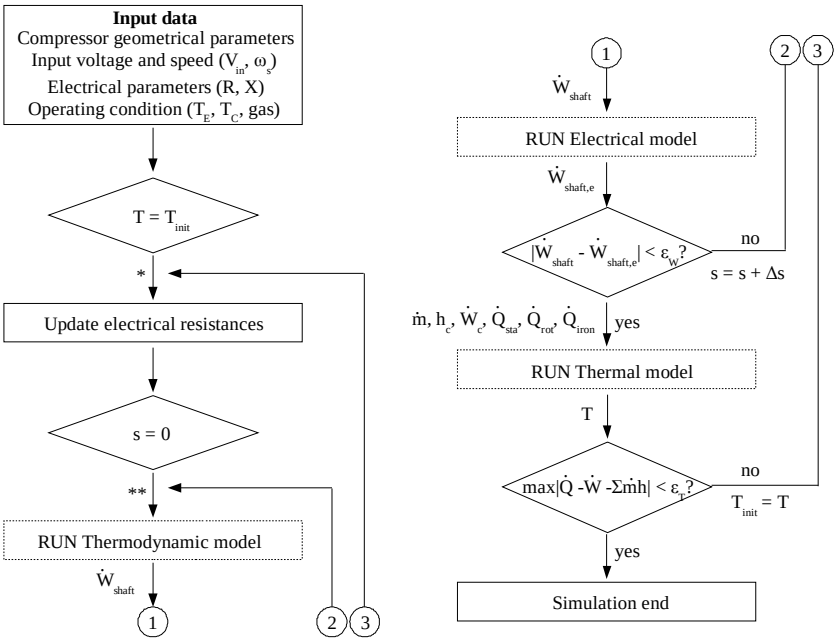

Figure 3: Coupled model algorithm.

6. RESULTS AND DISCUSSIONS

Numerical and experimental results of volumetric and isentropic efficiencies

$$\eta_v = \frac{\dot{m}}{\dot{m}_{th}}; \qquad \eta_s = \frac{\dot{W}_s}{\dot{W}_{in}} \tag{18}$$

as well as temperature distribution are shown in Figures 4 and 5, respectively. The results are presented for four operating conditions (Table 3) described by a pair of evaporating and condensing temperatures, suction line and environment temperatures, T_{evap}, T_{cond}, T_{sl} and T_{ee}, respectively. The condition OC1 is established by compressor testing standards, the conditions OC2 and OC3 represent high and low shaft power requirements and the condition OC4 is associated with high temperature profile. Global conductances between components were obtained from measurements under OC1 and maintained constant for the other three OCs.

Experimental results were obtained using a hot-cycle calorimeter facility designed to test compressors. On average, the actual compressor was tested 5 times under each operating condition, and the accuracy of the temperature measurements is within ±2.2ºC for a 90% confidence interval.

In terms of efficiency parameters, there is reasonable agreement between predictions and measurements. The good agreement for the isentropic efficiency is an indication of satisfactory predictions provided by the thermodynamic model ($\dot{W}_c$) and electrical model ($\dot{W}_{in}$). The largest deviations are noticed in the results for the condition OC4, i.e. difference of 9% for volumetric efficiency and 3% for isentropic efficiency.

Figure 5 shows that there is good agreement between predictions and experimental data of temperatures in the compressor components, with most differences smaller than ±5ºC. This agreement is also observed for condition OC4, in which the compressor temperature levels are clearly higher than those at the other operating conditions. The temperature of several components, such as the internal environment T_{ie}, housing, T_h and motor T_{mot}, seem to be almost insensitive to the operating conditions OC1, OC2 and OC3. However, the temperatures of other components vary significantly and are well predicted by the model. The model capability to correctly predict temperatures in the suction chamber, T_{sc}, and cylinder wall, T_w, is of major importance since both temperatures greatly affect the compression cycle.

Finally, the motor efficiency predicted by the coupled model simulation is compared to the theoretical motor efficiency at constant temperature. The motor efficiency is evaluated as a function of the shaft power, as depicted in Figure 6. First, it is interesting to note that the predictions of the coupled model are very close to a 80ºC constant temperature theoretical result. This is expected, since the results for the motor temperature are close to 80ºC (Figure 5). On the other hand, if a 25ºC constant temperature theoretical curve is used in such comparison, a difference of 2% is observed. This difference becomes even larger for high-load operating conditions. As can be seen, the coupled thermal-electrical model is able to predict the motor performance without requiring prior knowledge of its temperature.

Table 3: Operating conditions.

	T_{evap} (ºC)	T_{cond} (ºC)	T_{sl} (ºC)	T_{ee} (ºC)
OC1	-23.3	54.4	32.0	32.0
OC2	-10.0	60.0	32.0	32.0
OC3	-35.0	45.0	32.0	32.0
OC4	-35.0	70.0	40.0	43.0

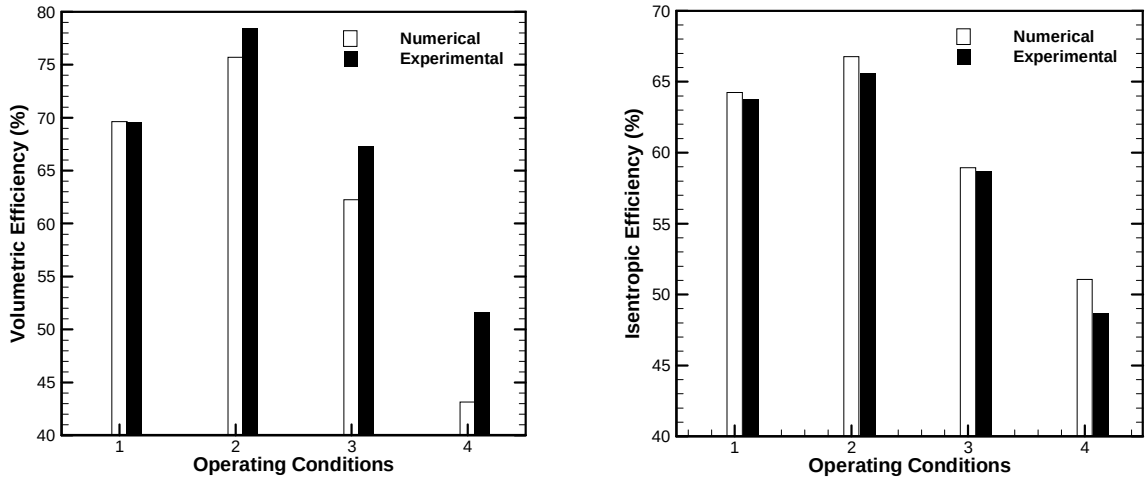

Figure 4: Volumetric and isentropic efficiencies.

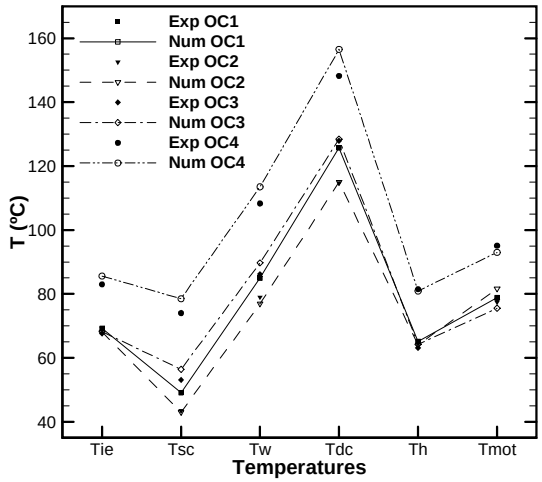

Figure 5: Temperature of compressor components.

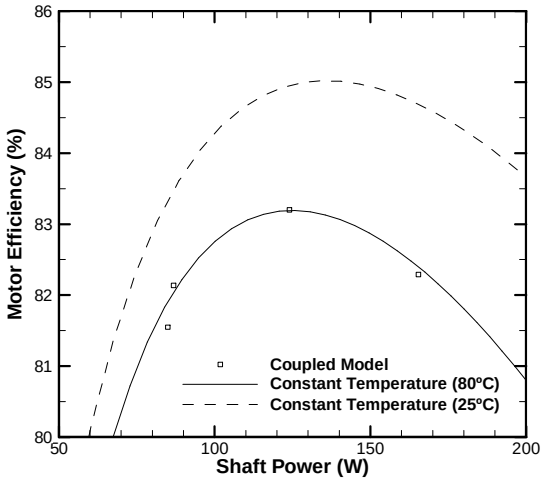

Figure 6: Motor efficiency.

7. CONCLUSIONS

This paper presented a lumped-parameter model formed by the coupling of thermodynamic, thermal and electrical models. The thermodynamic model is modeled through mass and energy balances in the compression chamber, whereas the thermal model is based on energy balances applied to the compressor components. The electrical model is represented by a motor equivalent circuit. The three models are solved in a coupled manner and predictions are provided for volumetric, isentropic and motor efficiencies, as well as temperature distribution. In general, reasonable agreement is observed between predictions and measurements. The model proposed herein is capable of accounting for the effect of motor losses on the compressor thermal profile, and vice-versa, without requiring experimental data or prior theoretical estimates for motor efficiency, torque and speed.

NOMENCLATURE

h	specific enthalpy	(J/kg)	s	slip ratio	(-)
I	electrical current	(A)	T	temperature	(K)
j	complex number indicator	(-)	UA	global conductance	(W/K)
$\dot{m}$	mass flow rate	(kg/s)	X	electrical reactance	(Ω)
$\dot{Q}$	heat transfer rate	(W)	$\dot{W}$	rate of work	(W)
R	electrical resistance	(Ω)	Z	electrical impedance	(Ω)

Subscript

suc	main flow through suction port	*dl*	discharge line
dis	main flow through discharge port	*h*	compressor housing
bsuc	backflow through suction port	*dt*	discharge tube
bdis	backflow through discharge port	*eh*	external side of housing
c	compression chamber	*ih*	internal side of housing
dc	discharge chamber	*mot*	motor
sc	suction chamber	*ie*	internal environment
dm	discharge muffler	*ee*	external environment
sm	suction muffler	*w*	cylinder wall
sl	suction line	*th*	theoretical

REFERENCES

Annand, W. J. D., 1963, Heat Transfer in the Cylinders of Reciprocating Internal Combustion Engines, *Proc. Inst. of Mech. Engineers*, 177, pp. 973- 996.

Birari, Y.V., Gosavi, S.S., Jorwekar, P.P., 2006, Use of CFD in Design and Development of R404a Reciprocating Compressor, *Proc. Int. Compressor Engrg. Conf. at Purdue*, Paper C072.

Cavallini, A., Doretti, L., Longo, G. A., Rosseto, L., Bella, B., Zannerio, A., 1996, Thermal Analysis of a Hermetic Reciprocating Compressor, *Proc. Int. Compressor Engrg. Conf. at Purdue*, pp. 535- 540.

Chikurde, R. C., Loganathan, E., Dandekar, D. P., Manivasagam, S., 2002, Thermal Mapping of Hermetically Sealed Compressors Using Computational Fluid Dynamics Technique, *Proc. Int. Compressor Engrg. Conf. at Purdue*, Paper C6-4.

Eltom, A. H., Moharari, N. S., 1991, Motor Temperature Estimation Incorporating Dynamic Rotor Impedance, *IEE Transactions on Energy Conversion*, Vol. 6, No 1,pp. 107-113.

Fitzgerald, A. E., Kingsley Jr., C., Umans, S. D., 2003, Electric Machinery, Mcgraw-Hill Companies, Inc., 6th Ed.

He, Z., Xing, Z., Chen, W., Wang, X., 2013, Thermal and Hydraulic Analysis on the Flow around the Motor in Semi-Hermetic Twin Screw Refrigeration Compressors, *App. Thermal Engrg. 58*, pp. 114-124.

Hrabovcova, V., Kalamen, L., Sekerak, P., Rafajdus, P., 2010, Determination of Single Phase Induction Motor Parameters, *SPEEDAM Int. Symp. on Power Electronics, Elec. Drives, Automation and Motion*, pp. 287–292.

Huai, Y., Melnik, R. V. N., Thogersen, P. B., 2003, Computational Analysis of Temperature Rise Phenomena in Electric Induction Motors, *App. Thermal Engrg.23*, pp. 779-795.

Hwang, C. C., Wu, S. S., Jiang, Y. H., 2000, Novel Approach to the Solution of Temperature Distribution in the Stator of an Induction Motor, *IEE Transactions on Energy Conversion*, Vol. 15, No 4, pp. 401-406.

Lemmon, E.W., Mclinden, M.O., Huber, M.L., 2002, REFPROP, Version 7.0, NIST.

Li, W., Cao, J., Zhang, X., 2010, Electrothermal Analysis of Induction Motor with Compound Cage Rotor Used for PHEV, *IEE Transactions on Industrial Electronics*, Vol. 57, No 2, pp. 660-668.

Lilie, D. E. B., Ferreira, R. T. S., 1984, Evaluation of the Leakage through the Clearance between Piston and Cylinder in Hermetic Compressors, *Proc. Int. Compressor Engrg. Conf. at Purdue*, pp. 1-6.

Lopes, M. N., Prata, A. T., 1997, Dynamical Behaviour of Reed Valves under Periodic Flow, COBEM 1138, *Proc. XIV Cong. Br. de Eng. Mec.* (CD-ROM), Bauru (in Portuguese).

Mellor, P. H., Roberts, D., Turner, D. R., 1991, Lumped Parameter Thermal Model for Electrical Machines of TEFC Design, *IEE Proceedings-B*, Vol. 138, No 5, pp. 205-218.

Meyer, W. A., Thompson, H. D., 1990, An Analytical Model of Heat Transfer to the Suction Gas in a Low-Side Hermetic Refrigeration Compressor, *Proc. Int. Compressor Engrg. Conf. at Purdue*, pp. 898-907.

Ooi, K.T., 2003, Heat Transfer Study of a Hermetic Refrigeration Compressor, *App. Thermal Engrg.*,V.23, pp. 1931–1945.

Peruzzi, F., Bacci, V., Scandurra, G., 1980, EER Improvement on a Reciprocating Hermetic Compressor, *Proc. Int. Compressor Engrg. Conf. at Purdue*, pp. 1-7.

Raja, B., Sekhar, S. J., Lal, D. M., Kalanidhi, A., 2003, A Numerical Model for Thermal Mapping in a Hermetically Sealed Reciprocating Refrigerant Compressor, *Int. J. of Refrigeration 26 (6)*, pp. 229-236.

Ribas Jr., F. A., 2007, Thermal Analysis of Reciprocating Compressors, *Int. Conf. on Compressors and Their Systems*, London, pp. 277-287.

Rigola, J., Pérez-Segarra, C. D., Oliva, A., 2000, Advanced Numerical Simulation Model of Hermetic Reciprocating Compressors. Parametric Study and Detailed Experimental Validation, *Proc. Int. Compressor Engrg. Conf. at Purdue*, pp. 23-30.

Sanvezzo Jr., J., Deschamps, C. J., 2012, A Heat Transfer Model Combining Differential and Integral Formulations for Thermal Analysis of Reciprocating Compressors, *Proc. Int. Compressor Engrg. Conf. at Purdue*, paper 1343.

Soedel W., 2007, Sound and Vibration of Positive Displacement Compressors, CRC Press, pp. 324.

Todescat, M.L., Fagotti, F., Prata, A.T., Ferreira, R.T.S., 1992, Thermal Energy Analysis in Reciprocating Hermetic Compressors, *Proc. Int. Compressor Engrg. Conf. at Purdue*, pp. 1417-1428.

Ussyk, M.S., 1984, Numerical simulation of hermetic reciprocating compressors, *M. Sc. Thesis*, Federal University of Santa Catarina (in Portuguese).

ACKNOWLEDGEMENT

The material discussed herein forms part of a joint technical-scientific program of the Federal University of Santa Catarina and EMBRACO. The authors also acknowledge the support provided by EMBRACO and CNPq (Brazilian Research Council) through Grant No. 573581/2008-8 (National Institute of Science and Technology in Refrigeration and Thermophysics).